



NUMERICAL STUDY ON THE CAVITATION NOISE OF MARINE SKEW PROPELLERS

Agung Purwana¹, I. Made Ariana², Wisnu Wardhana³

¹Department of Marine Engineering, Faculty of Marine Technology, Institut Teknologi Sepuluh Nopember (ITS), Surabaya 60111, Indonesia, agpurwana@gmail.com

²Department of Marine Engineering, Faculty of Marine Technology, Institut Teknologi Sepuluh Nopember (ITS), Surabaya 60111, Indonesia, ariana@its.ac.id

³Department of Ocean Engineering, Faculty of Marine Technology, Institut Teknologi Sepuluh Nopember (ITS), Surabaya 60111, Indonesia, wisnu.wardhana2@yahoo.com

Abstract:

In this study, numerical simulations on the noise of the underwater marine propeller for different pressures, skew angles, and performance conditions are investigated. The study has been carried out for the prediction of cavity and noise cavitation characteristics of the propeller. The blade sheet cavitation created by an underwater propeller is then evaluated using numerical analysis. The cavitation and cavity around marine propellers were predicted using MRF (Multiple Reference Frame) techniques. The simulation uses the Reynolds Averaged Navier-Stokes (RANS) formulation with the turbulence model $k-\omega$ Shear Stress Transport and the Fast Fourier Transform. The FW-H equation is used to measure far-field radiation under various operating conditions. The simulation is carried out to present that the pressure and skew propeller angles have an effect on the form and area of the cavity, as well as cavitation noise. The noise characteristics at various positions of hydrophones and speeds of the marine propeller are presented. The 3D model of B-series marine propeller with $D=250$ mm, $Z=4$, $P/D=1.0$, $AE/AO=0.55$, skew angles of 16, 35, 53, and 72 degrees at advance coefficient, $J=0.221$, is used for the simulation.

Keywords: Numerical simulation, cavitation, noise, marine propeller.

NOMENCLATURE

D	Propeller diameter (m)	KT _{Prop}	Propeller thrust coeff., $T_{Prop} / \rho n^2 D^4$
Z	Number of Blades	10KQ	Propeller torque coeff., $10Q / \rho n^2 D^5$
n	Propeller rotational speed (rps)	J	Propeller advance coeff., V_A / nD
V _A	Propeller advance speed, in the direction of carriage motion (m/s)	η_{Prop}	Propeller efficiency, $J / 2\pi \times (KT_{Prop} / KQ)$
T	Propeller thrust (N)	Re	Reynold number of a characteristic radius (0.75R).
Q	Propeller torque (Nm)	σ	Cavitation number $\sigma = \frac{v}{0.5\rho N^2 D^2}$

$$(R_{\sigma})_{0.75R} = \frac{C_{0.75R} \sqrt{[V_A^2 + (0.75 \pi n D)^2]}}{v}$$

1. Introduction

Currently, the research characteristics and acoustics of marine propellers for ships are important and burning topics discussed. Based on the interests of various stakeholders in the environment and habitats within the sea, IMO (International Maritime Organization) issued new regulations on ocean noise. The sound generated by the propeller is often disturbing the habitat's comfort in the ship and underwater. This paper only considered cavitating marine propeller-induced noise and propeller cavity using numerical simulation. Researchers specifically investigated the performance and noise of marine propellers using numerical simulations such as Williams and Hawkins (1969) published acoustic predictions with the method for calculation noise an arbitrary body moving in a fluid are still adopted in hydro-acoustics predicted by this available method in computational

numerical practice. Non-cavitation noise of the underwater propeller is numerically investigated using time-domain acoustic analogy and boundary element method and Williams–Hawking’s formulation to predict the far-field acoustics. Noise prediction results are presented for single propeller and ducted propeller by Seol et.al (2002). To predict the far-field acoustics, Seol et al (2002). perform a numerical study on the non-cavitating and blade sheet cavitation noises of the underwater propeller using time-domain acoustic analogy and Williams–Hawking’s formulation. Salvatore and Ianniello (2003) predicted cavitation sheet propeller noise transiently with a hydrodynamic model coupled with a hydro-acoustics model in non-uniform inviscid flow based on the Williams-Hawking’s equation corresponding to the Bernoulli equation model. Barbarino and Casalino (2012) predicted and validated analytically and numerically for the trailing-edge noise spectrum in the frequency domain from a flat plate from a NACA-0012 airfoil. Ozden et. al. investigated a numerically for the INSEAN E1619 submarine propeller radiated noise in open water and behind a generic DARPA sub-off using Reynolds Averaged Navier-Stokes (RANS) and Williams-Hawking equation. Kawamura et al. (2004) compared various turbulence models for predicting the performance of a conventional propeller in open water. Li (2006) used the k- ω turbulence model to estimate the open water characteristics of a highly skewed model propeller, and the analysis was then validated using experimental data. The author continues previous research about numerical simulation for predicting the performance and noise of marine propellers (Agung et al., 2017) and cavitation noise of symmetrical blade submarine propellers (Agung et al., 2018). The cavitation phenomenon of the sheet in the form of a large bubble on the surface of the propeller blade generates low-frequency noise by forming regions I and II in the general sound spectrum of the cavitation propeller described in Figure 1. It is important to analyze accurately cavitation sounds that are the main source of propeller noise (Seol et al., 2005). The study presents a numerical analysis of the noises of the propeller for different performance conditions. This paper has been carried out for the prediction of cavity and noise propeller cavitation characteristics of submarine propellers using numerical simulation. The blade cavitation noise generated by an underwater submarine propeller is analyzed numerically.

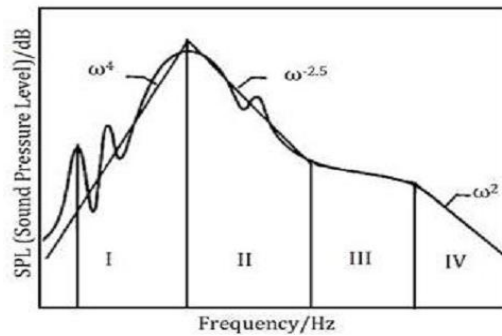


Fig. 1: Cavitation noise frequency ranges for underwater propellers (Seol et al., 2005)

2. Numerical Simulation

This work is carried out using numerical simulation, which has a built-in marine propeller hydrodynamic performance coefficient (KT, Kq, η) corresponding to the advance coefficient (J) and Reynolds number (Re) equation. The flow field is studied using the finite volume method (FVM) in this paper, and the propeller computation domain is the cylindrical form surrounding the propeller, in which a rotating cylinder with a diameter sufficiently larger than the propeller’s diameter enfolds the propeller inside the centre of the cross-section and allows fluids to pass through the model. The rotating zone is settled by means of the Moving Reference Frame (MRF) as presented in Figures 3 and 4, and then time-dependent flow field data is utilized as input for the Williams-Hawking’s formulation to predict far-field acoustics. Noise characteristics are estimated and measured based on noise and conditions sources. The developed flow solver is applied to the model propeller in a uniform inflow. The simulation is carried out utilizing the W-H formula (Williams Hawking’s Equation) as previously discussed. The Navier-Stokes and continuity equation have been manipulated and derived into W-H Equations for nonhomogeneous wave equations (Sauer and Schnerr, 2000). The following is the governing equation for continuity used for numerical calculations.

$$\frac{\partial \rho}{\partial t} + \frac{\partial}{\partial x_i} (\rho v_i) = 0 \tag{1}$$

Where x_i and v_i are the tensor form of velocities and axial coordinates. And the momentum equation becomes:

$$\frac{\partial(\rho v_i)}{\partial t} + \frac{\partial(\rho u_i u_j)}{\partial x_j} = -\frac{\partial p}{\partial x_i} + \frac{\partial}{\partial x_j} \left[\mu \left(\frac{\partial u_i}{\partial x_j} + \frac{\partial u_j}{\partial x_i} - \frac{2}{3} \delta_{ij} \frac{\partial u_l}{\partial x_l} \right) \right] + \frac{\partial}{\partial x_j} (-\rho u_i' u_j') \tag{2}$$

Where δ_{ij} is Kronecker Delta and $-\rho u_i' u_j'$ are the unknown Reynolds stresses.

$$\frac{1}{\alpha_0} \frac{\partial^2 p'}{\partial t^2} - \nabla^2 p' = \frac{\partial^2}{\partial x_i \partial x_j} \{T_{ij} H(f)\} - \frac{\partial}{\partial t} \{ [P_{ij} n_j + \rho u_i (u_n - v_n)] \delta(f) \} + \frac{\partial}{\partial t} \{ [\rho_0 v_n + \rho (u_n - v_n)] \delta(f) \} \tag{3}$$

P_{ij} denotes the compressive stress tensor, p' is defined as the sound pressure at the far-field calculated by $p' = p - p_0$. $H(f)$ is Heaviside function, v_i is surface velocity component in the x_i direction, T_{ij} is Lighthill stress tensor, v_n is surface velocity component normal to the surface u_i is fluid velocity component in the x_i direction, u_n is fluid velocity component normal to the surface $f=0$, $\delta(f)$ is Dirac delta function. The free-space Green's function is used to find the solution to the above Equation. For the study of turbulence modeling with good performance on wall-bounded flow limit layer used turbulence model of SST k- ω . (Li, 2006). Several numerical methods for the prediction of cavitation flow on propeller blades have been developed in the form of models with single-phase and multi-phase models with cavitation interface tracking. The multi-phase model is used in this paper to track liquid and gas. The cavitation model introduced by Yuan et al., (2001) was used in this study to track cavitation. This model is adopted based on the approach that the mixture contains a large number of spherical bubbles. The mass exchange rate is then determined using a simplified Rayleigh-Plesset equation-based model for bubble growth. As a consequence, non-equilibrium effects should be taken into account.

$$R_e = \frac{\rho_v \rho_l}{\rho_m} \alpha (1 - \alpha) \frac{3}{R_B} \sqrt{\frac{2(p_v - p)}{\rho_l}} \quad R_c = \frac{\rho_v \rho_l}{\rho_m} \alpha (1 - \alpha) \frac{3}{R_B} \sqrt{\frac{2(p - p_v)}{\rho_l}} \tag{4}$$

With R_b being the bubble radius given as:

$$R_B = \left(\frac{\alpha}{1 - \alpha} \frac{3}{4\pi} \frac{1}{n_b} \right)^{\frac{1}{3}} \tag{5}$$

The number of vapor bubbles per volume of liquid is the only constant that must be calculated (n). According to Yuan et al., (2001), a value of 1.51014 nuclei/m³ water is in good agreement with experimental observations by Roosen, et al., (1996). In the present calculation, we used unsteady numerical simulation via a Coupled algorithm with a second-order implicit pressure-based solver. Least Squares Cell-Based is used for gradient and PRESTO for pressure discretization. The k- ω -SST model was used, and the second-order upwind scheme was selected as the discretization scheme in all cases for cavitating turbulent flows around a highly skewed model marine propeller has been conducted to predict the propeller performance. This study has been carried out for the prediction of cavity and noise. The propeller cavitation characteristics of the propeller using numerical simulation are compared with those calculated by Burrill Diagram (Burrill and Emerson, 1978).

3. B-Series Propeller Modelling

The B4.55 propeller has been numerically calculated in open water condition. The Open water experiments were performed in the Wageningen towing tank. Results were presented by Troost (1938). The geometric particulars of the Propeller are furnished in Table 1 whereas the 3D models of the propeller are shown in Fig. 2. The mesh of the B4.55 Propeller with a skew of 16 degree is shown in Fig. 3.

Table 1: Propeller main dimension

Main Dimension	B.4.55			
Number of Blades, Z	4			
Diameter (m)	0.25			
Pitch Ratio at 0.7R	1.0			
AE/A0	0.55			
Hub/Diameter Ratio	0.21			
Rake	15°			
Skew	16°	35°	53°	72°
Direction of rotation	Right			

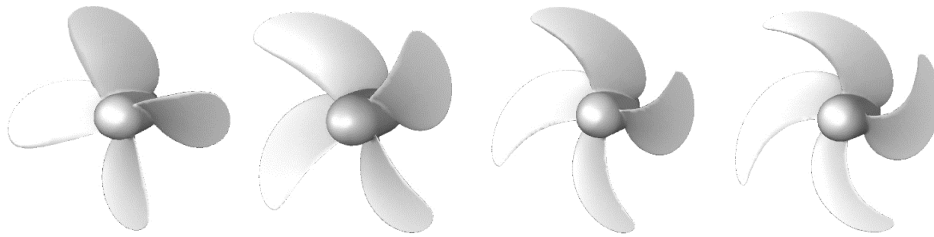


Fig. 2: 3D model of B4.55 propeller with a skew of 16, 35, 53 and 72 degree (from left to right)

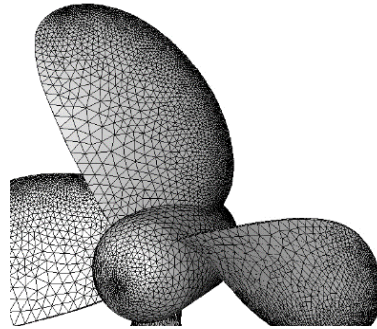


Fig. 3: Mesh of B4.55 propeller with a skew of 16 degree

In modeling flow around the propeller, the homogeneous fluid flow region is numerically divided into dynamic and stationary zones as illustrated in Fig. 4. Using the Coriolis acceleration term in the equation, the dynamic frame is simulated by the propeller rotation. The diameter of the propeller (D) is used as a reference relating to the frame dimension. The size of the static frame diameter is $3D$ with an overall length of $7D$, with a distance of $2D$ from the inlet side and $5D$ from the outlet side. The size of the computational domains in this study is used based on the authors' previous work and some other numerical simulation works on marine propellers.

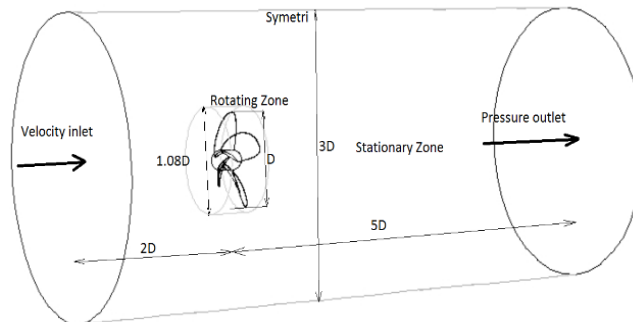


Fig. 4: 3D Computational domain around propeller (rotating and stationary zone) and boundary conditions.

In this study, the propeller open water characteristics are calculated at advance coefficient, $J = 0.221$ with 7.5rps . A mesh independence study was performed using 1291096 and 2959091 cells. Table 2 shows open water characteristics of the propeller for different mesh sizes. Unstructured tetrahedral cells are used in stationary blocks and spin for vane cells and prisms with a size of $0.00255792D$ selected for the boundary layer at the vane surface as shown in Fig. 3. Therefore, the number of cells selected for the blades is 2.96 million.

Table 2: The relative error of Numerical Simulation results with respect to the experiments for grid dependency study.

Number of cells	KT (%)	10KQ (%)	η (%)
919281	3.278	-0.289	3.642
1291096	1.504	-1.226	2.846
2959091	-0.547	-2.29	-1.73

4. Noise Prediction in Open Water

Noise characteristics of the propeller in open water condition were computed transiently at $J=0.221$ with the propeller rotational speed of 29 rps. This study presents the cavitation noise to find the range of Sound Pressure Levels (SPLs), as well as its development and the effect of cavitation noise on the SPL's. In Table 3, V_a is the axial velocity of the flow, N denotes the rotational speed, ρ is the density of water, a_0 is the sound velocity and P_{ref} is the reference underwater pressure. P is the pressure of the flow past the propeller. In this numerical simulation, 3 hydrophones are used to extract SPLs. The position of the hydrophone and its coordinates are presented in Fig. 5 and Table 4 respectively.

Table 3: Parameters of flow and acoustic conditions

J	V_a (m/s)	N (rps)	ρ (kg/m ³)	a_0 (m/s)	Pref (Pa)	P (Pa)
0.221	1.601	29	998.2	1500	10^{-6}	50,75, 85 and 120kPa

Table 4: Coordinates of Hydrophones

Name	X-Coordinate (m)	Y-Coordinate (m)	Z-Coordinate (m)
Hydrophone 1	1.0	0.375	0
Hydrophone 2	1.0	0	0.375
Hydrophone 3	1.0	0	0

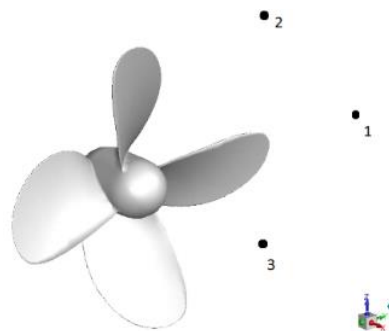


Fig. 5: Position of Hydrophones for Numerical Simulation.

5. Propeller Performance

The predicted noise generated by the propeller is directly related to the precision of the pressure on the blade surface. Fig. 6 shows the volume fraction vapor distribution on the backside of the propeller with a skew of 16 degrees at $J= 0.221$ for various pressures (50, 75, 85kPa). Also, the Iso-surface volume fraction vapor 0.199 distribution on the backside of the propeller at an advance coefficient of $J= 0.221$ is shown in Fig. 7. It shows the cavity volume of vapor fraction which becomes smaller with the increase of the pressure. The values of thrust and torque at given advanced ratios were calculated and captured very well using RANS equations. Tables 5-7 show the comparison of thrust and torque of the propeller with respect to the advance coefficient, $J=0.221$. The hydrodynamic characteristics of the propeller at constant rotation, $N=29$ rps are shown in Table 6 for different pressures of the fluid flowing past the propeller. The computed values of thrust coefficient (K_T), the torque coefficient (K_Q) and efficiency (η) are less than the experimental ones for pressures, $P=50, 75, 85$ kPa. With the increase of pressure, the difference between computed and experimental values decreases. However, for $P=120$ kPa, the thrust coefficient almost equals to experimental value and the torque coefficient becomes larger.

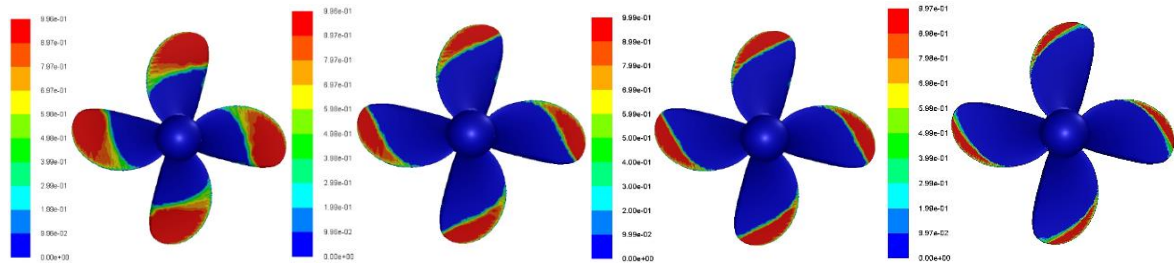


Fig. 6: Volume fraction vapour distribution on back side of the propeller at $J = 0.221$, $N=29$ rps, $v=1.601$ m/s, left: 50, 75, 85 and right: 120kPa

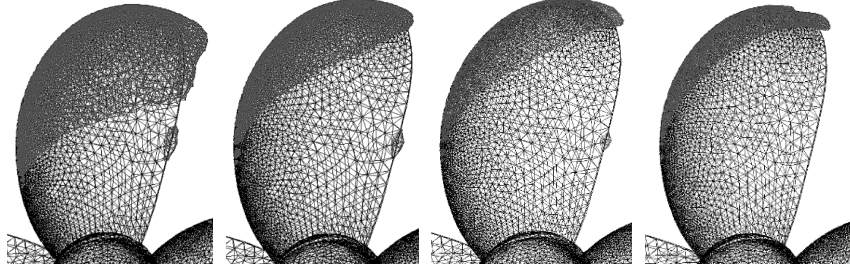


Fig. 7: Iso Surface volume fraction vapour 0.199 distribution on back side of the propeller at $J = 0.221$ -29rps- $v=1.601$ m/s, left: 50 and 75kPa.- $v=1.601$ m/s, 50, 75, 85 and right: 120kPa

Table 5: B series data for propeller

B series data			
J	Kt	10Kq	η
0.221	0.365	0.522	0.246

Table 6: The Numerical Simulation results and error with respect to the B series data for propeller skew 16 degrees at $J=0.221$ -50, 75, 85 and 120kPa

N (rps)	Simulation								Pressure (k Pa)
	T (N)	Q (Nm)	Kt	10Kq	η	ΔKT (%)	$\Delta 10KQ$ (%)	$\Delta \eta$ (%)	
29	933.5816	37.519	0.285	0.458	0.2185	21.918	12.261	11.179	50
29	1011.32	38.779	0.308	0.473	0.2289	15.616	9.387	6.951	75
29	1053.306	40.326	0.321	0.492	0.2293	12.055	5.747	6.789	85
29	1194.778	44.794	0.364	0.546	0.2342	0.274	-4.598	4.797	120

Evaluation of the cavitating propeller using Burrill’s Diagram is shown in Fig. 10. The results of numerical simulations of cavitation propellers with pressures of 50kPa (red line), 75kPa (yellow line), 85kPa (green line) and 120kPa (brown line) were compared with cavitation experimental results by Burrill (1978). For all pressure variations, there is more than 10% back cavitation. This is in accordance with the simulation results shown in Fig. 9. Table 7 shows the numerical simulation results and comparison to the Burrill Diagram data for the propeller for the pressure of 50, 75, 85, and 120kPa.

Table 7: The Numerical simulation results and comparison to the Burrill Diagram data for the propeller for the pressure of 50, 75, 85 and 120kPa.

Result	50 kPa	75 kPa	85 kPa	120 kPa
A_p (m ²)	0.022613			
Vapor press(e) (Pa)	3540(27°C)			
qT	128020.83			
A_p (m ²)	0.022613			
qT	128020.83			
P-e (Pa)	46460	71460	81460	116460
Tc	0.322	0.349	0.364	0.413
Local Cav.Number	0.363	0.558	0.636303	0.9097
T (N)	933.58163	1011.3177	1053.3063	1194.7778

The propeller for the pressure of 50 kPa, rotated at 29rps possesses less efficiency than the propeller for the pressure of 75, 85, and 120 kPa at the same rotation. If the propeller is rotated with a high rotation of 29rps and the static pressure around the propeller blade decreases resulting in a decrease in thrust coefficient, torque coefficient, and propeller efficiency. This is due to the phenomenon of cavitation. The performance of the propeller can be seen in Table 6 and Figs. 9-11. Figs. 11-12 show the volume fraction vapor distribution on the backside of the propeller with skews of 35, 53, and 72 degrees at $J = 0.221$ for the pressure of 75kPa.

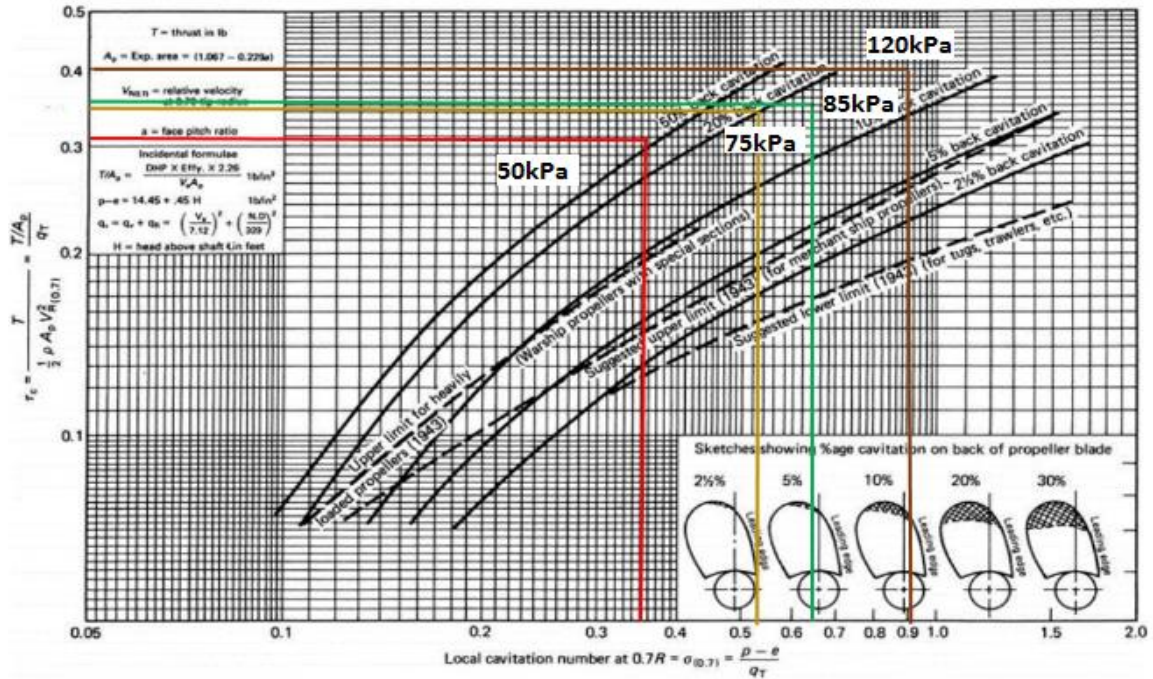


Fig. 8: Burrill Diagram graph for propeller with a skew of 16 degrees at $J = 0.221$ -29rps-50, 75, 85 and 120kPa.

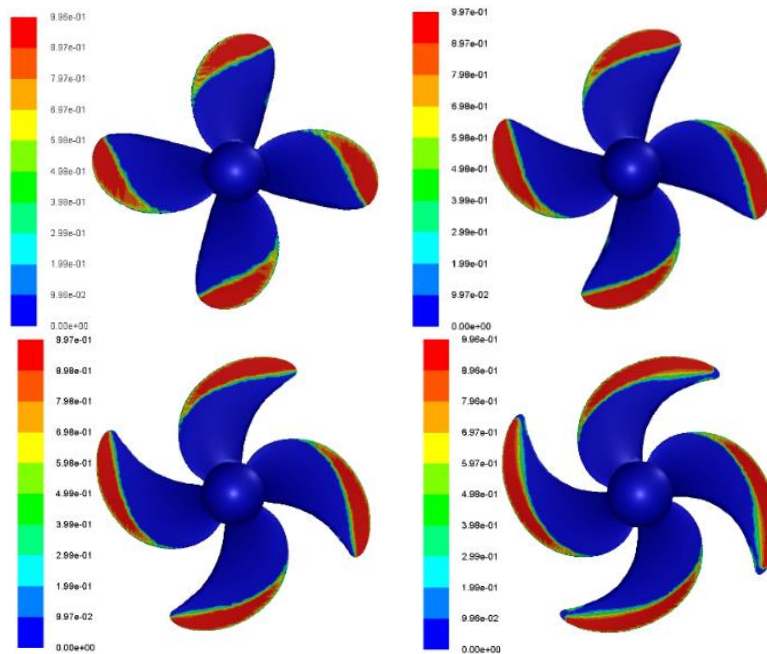


Fig. 9: Volume fraction vapor distribution on back side of the propeller a skew of 35, 53 (left) and 72 (right) degrees at $J = 0.221$ -29rps, $v = 1.601$ m/s, $P = 75$ kPa.

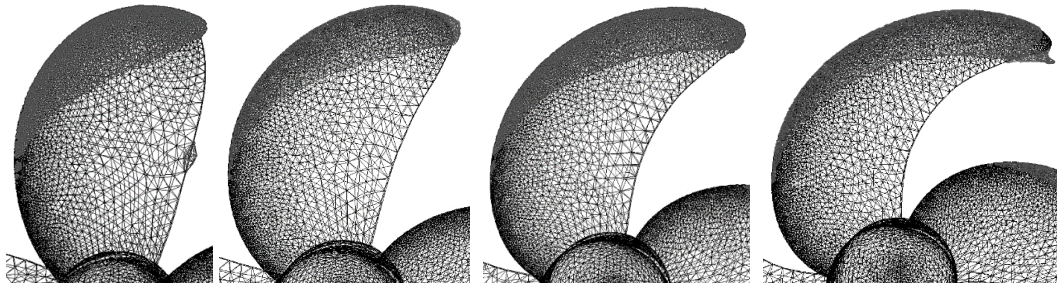


Fig. 10: Iso Surface volume fraction vapor 0.199 distribution on back side of the propeller skew: left: 16, 35, 53 and right: 72 degrees at $J = 0.221$ -29rps- $v=1.601$ m/s, 75kPa.

The propeller is rotated 29rps it produces a large thrust and torque but produces a smaller thrust coefficient, torque coefficient, and efficiency. This is caused by the phenomenon of cavitation. The performance of the propeller can be observed in Table 8. In the numerical simulation, the vapor volume fraction on the propeller with skews of 35 53 and 72 degrees decreases as compared to that with a skew of 16 degree as can be seen in Figs.11-12.

Table 8: The Numerical Simulation results and error with respect to the B series data for propeller skew 35, 53 and 72 degrees at $J=0.221$ -75kPa.

Skew degrees	N (rps)	Simulation							
		T (N)	Q (Nm)	Kt	10Kq	η	ΔKT (%)	$\Delta 10KQ$ (%)	$\Delta \eta$ (%)
35	29	1080.35	41.254	0.3294	0.5032	0.2303	9.73973	3.5977	6.542
53	29	1113.63	42.603	0.3396	0.5197	0.2298	6.9592	0.446	6.589
72	29	1170.09	44.659	0.3568	0.5448	0.2300	2.241	-4.358	6.492

6. Propeller Noise

The cavitation noise characteristics are expressed in accordance with the propeller blades under cavitation operating conditions as a noise source.

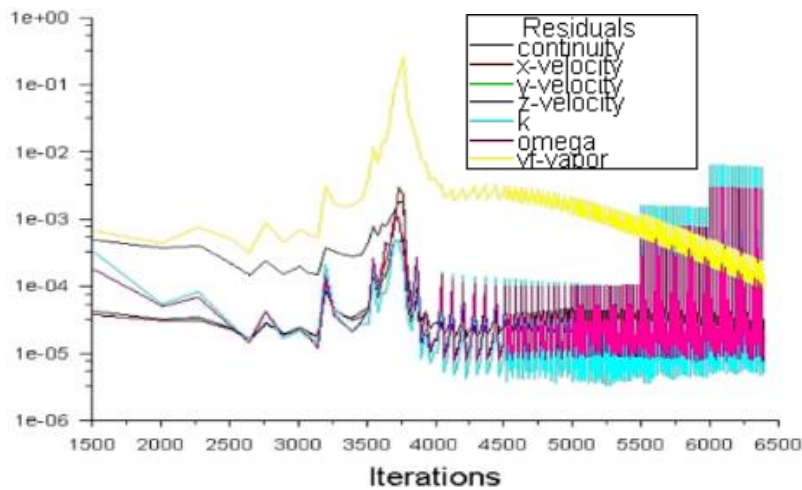


Fig. 11: Convergence graph at $J= 0.221$ -29rps.

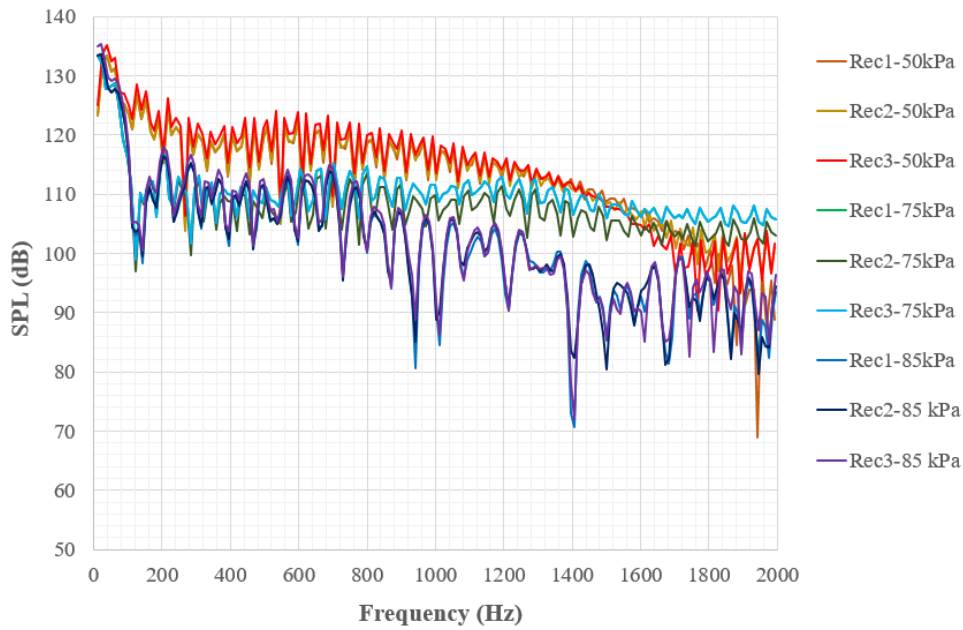


Fig. 12: Acoustic prediction graphs SPLs (dB) hydrophone 3 Pref (Pa) = 10^{-06} at $J = 0.221-29\text{rps-v} = 1.601 \text{ m/s}$ with a pressure of 50kPa, 75kPa, and 85kPa.

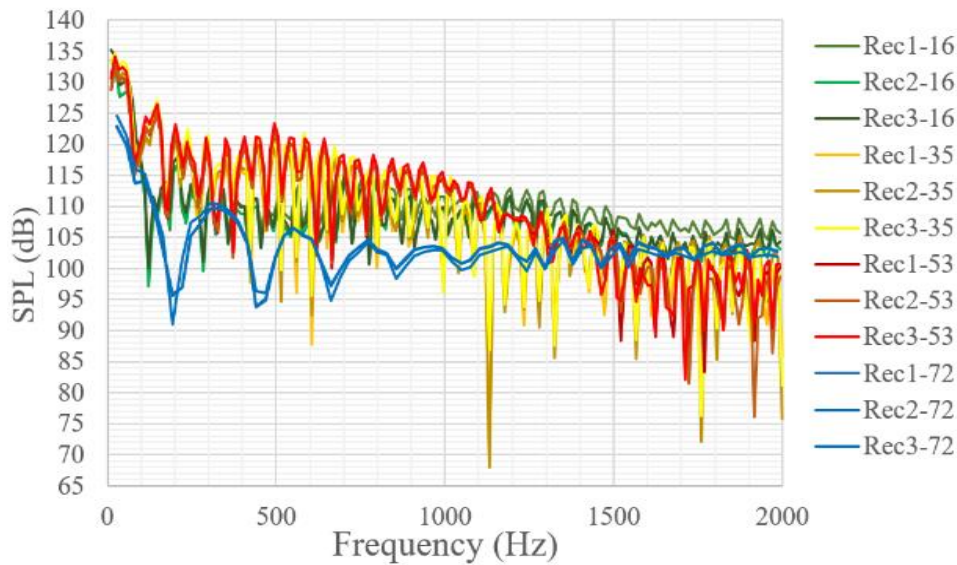


Fig. 13: Acoustic prediction graphs SPLs (dB) propeller skew 16, 35, 53 and 72, hydrophone 1, 2 and 3 Pref (Pa) = 10^{-06} at $J = 0.221-29\text{rps-v} = 1.601 \text{ m/s}$ with pressure 75kPa.

According to the results, cavitation noise is incepted by increasing flow velocity and propeller rotation speed. The graph below illustrates a history of convergence of the propeller sound pressure levels. The difference between the previous and present values in the range of 1×10^{-4} is considered as the convergence criterion. The acoustic graphs in Figs. 12-13 show the Sound Pressure Levels (SPLs) of the propeller generated from various receivers that are placed at various positions for different operating conditions, flow velocity and propeller rotational speed. The result of experiments shows that the SPL increase with the higher cavity at $J=0.221$, $N=29\text{rps}$, $P=50\text{kPa}$ with a skew of 16 degree as shown in Fig.12. The result of experiments shows that the SPL decreases with the smaller cavity at $J=0.221$, $N=29\text{rps}$, $P=75\text{kPa}$ with a skew of 72 degree as observed in Fig.13. This phenomenon is caused by the increase of the rotational speed of the propeller. Higher rotational speed of the propeller and the fluids that flow through the propeller cause turbulence and cavitation which generate a higher propeller noise. According to Bernoulli's Law, the flow of the water through the propeller blades causes

higher pressure in the face than in the back of the propeller. As the rotation of the propeller increases, this pressure difference becomes much higher. Low pressure induces bubbles due to the boiling of water in the back of the propeller. Cavitation with cavity size is proportional to the dimension of flow characteristics as shown in Figs. 11-13. The potential of noise generated during the collapse of cavitation bubbles is examined in this paper. The hydrodynamic or acoustic fluid pressure varies greatly and changes very rapidly during cavitation. Bubbles with water vapor collapses are often changing and short-lived and generate high-intensity acoustic pressure. When the maximum radius reaches, the bubble-cavitation is at a higher-pressure area then the bubble becomes collapsed. The shock waves generated and an increase in bubble velocity that exceeds the speed of the sound of the fluid is the result of bubbles collapsing and explosions in the liquid. Evaporated bubbles that are faster can produce more noise and damage than cavitation bubbles of gas containing non-condensing gases. Cavitation is not desirable on the marine propeller because it can cause damage to the surface of the blade, causing noise and vibration, and leading to a reduction in efficiency.

7. Conclusions

This paper investigated the hydrodynamic and noise phenomenon of a propeller in cavitating conditions using RANS equation solver. The result of this paper shows that the numerical findings are in good agreement with the experimental data. The experiment has been done at the propeller speed of 29 rps with flow velocity of 1.601 m/s for noise prediction. The result of experiments shows that the overall SPLs for Hydrophone 3 with skews of 16, 35, 53 degrees is higher than Hydrophone 3 and 2 with a skew of 72 deg. since the higher turbulence and cavitation in the location of Hydrophone 3. The noise of the propeller with a skew of 53 deg. is higher than the propeller with skews of 16, 35 and 72 degrees. The ranges of SPLs increase as the rotational speed of the propeller increases, since both parameters affect the increase of turbulence and cavitation. The findings can be utilized to optimize the operating parameter of the derivate pattern of noise radiation in an underwater vehicle.

Acknowledgment

The Ministry of Research, Technology and Higher Education of Indonesia has financially supported this works. The simulation work was supported by the Chemical Engineering Department of Institut Teknologi Sepuluh Nopember Surabaya.

References

- Barbarino, M., Casalino, D. (2012): Hybrid analytical/numerical prediction of propeller broadband noise in time domain. *Int. Jour. of Aeronautics*, 11(2), pp.157-175. <https://doi.org/10.1260/1475-472X.11.2.157>
- Burrill, L.C., Emerson, A. (1978): Propeller cavitation: further tests on 16 in. propeller models in the King's College Cavitation Tunnel. *Trans. NECIES*, 195.
- Kawamura, T., Watanabe, T., Takekoshi, Y., Maeda, M., Yamaguchi, H. (2004): Numerical simulation of cavitating flow around a propeller, *Journal of the Society of Naval Architects*, 195. https://doi.org/10.2534/jjasnaoe1968.2004.195_211
- Li, D. Q. (2006): Validation of rans predictions of open water performance of a highly skewed propeller with experiments. *Journal of Hydrodynamics*, 18(3), Supplement, pp.520-528. [https://doi.org/10.1016/S1001-6058\(06\)60106-6](https://doi.org/10.1016/S1001-6058(06)60106-6)
- Ozden, M. C., Gurkan, A. Y., Özden, Y. A., Canyurt, T. G., Korkut, E. (2014): Underwater radiated noise prediction for a submarine propeller in different flow conditions, A. Yücel Odabaşı Colloquium Series 1st International Meeting - Propeller Noise & Vibration 6th - 7th November 2014, Istanbul, Turkey.
- Purwana, A., Ariana, I. M., Wardhana, W., Widhi, H.D. (2017): Performance and noise prediction of marine propeller using numerical simulation. *The 3rd International Seminar on Science and Technology*, 3rd August 2017, Postgraduate Program, Institut Teknologi Sepuluh Nopember, Surabaya, Indonesia.
- Purwana, A., Ariana, I. M., Wardhana, W., Widhi, H.D. (2018): Numerical study on cavitation noise of symmetrical blade submarine propeller. *1st Maritime Safety International Conference (MASTIC)*.
- Roosen, P., Unruh, O. and Behmann, M. (1996): Investigation and modeling of the transient behavior of cavitation phenomena with single and multi-component fuels in fast flow nozzle, Report of the Institute for Technical Thermodynamics, RWTH Aachen Univ. of Technology (in German).
- Salvatore, F. and Ianniello, S. (2003): Preliminary results on acoustic modeling of cavitating propellers. *Comp. Mechanics*, 32, pp.291-300. <https://doi.org/10.1007/s00466-003-0486-4>

- Sauer, J. and Schnerr, G.H. (2000): Unsteady cavitating flow-a new cavitation model based on a modified front capturing method and bubble dynamics, Proceeding of FEDSM2000-11095, 2000 ASME Fluids Engineering Summer Conference, June 11-15, Boston, Massachusetts, USA
- Seol, H., Suh, J.C. and Lee, S. (2002): Prediction of non-cavitating underwater propeller noise. *J. Sound and Vibration*, 257(1), pp.131 -156. <https://doi.org/10.1006/jsvi.2002.5035>
- Seol, H., Suh, J.C. and Lee, S. (2005): Development of hybrid method for the prediction of underwater propeller noise, *J. Sound and Vibration*, 288(1), pp.345-360. <https://doi.org/10.1016/j.jsv.2005.01.015>
- Troost, L. (1938): Open water test series with modern propeller forms, *Trans North East Coasts Inst. of Engineers and Shipbuilders*, p. 321. N.S.M.B. Publ. No.33. (A4.40, B4.40, B4.55)
- Williams, J. E. F, Hawkins, D. L. (1969): Sound generation by turbulence and surfaces in arbitrary motion. *Philosophical Transactions of the Royal Society of London, Series A, Mathematical and Physical Sciences*, 264: 321 -342. <https://doi.org/10.1098/rsta.1969.0031>
- Yuan, W., Sauer, J. and Schnerr, G.H. (2001), Modeling and computation of unsteady cavitation flow in injection nozzles, *Mechanics and Industries*, 2, 383-394. [https://doi.org/10.1016/S1296-2139\(01\)01120-4](https://doi.org/10.1016/S1296-2139(01)01120-4)